



Wave-Shaped Piezoelectric Nanofiber Membrane Nanogenerator for Acoustic Detection and Recognition

Fan Xu¹ · Jiang Yang¹ · Ruizhi Dong² · Hanxiao Jiang¹ · Conghuan Wang¹ · Weilin Liu¹ · Zaixiu Jiang² · Xiaoqing Zhang³ · Guodong Zhu¹

Received: 29 May 2021 / Accepted: 24 July 2021 / Published online: 21 September 2021
© Donghua University, Shanghai, China 2021

Abstract

With the rapid development of internet of things and wearable electronics, how to conveniently power uncountable sensors remains a huge challenge. Energy harvesting strategy is suggested to collect and convert environmental energies into electrical energy. Thereinto, piezoelectric polymers are utilized as flexible harvesters to convert mechanical energy. The latter widely distributes in both our daily life and industrial environment. Intrinsic piezoelectric property further drives piezoelectric polymers to construct flexible self-powered strain sensors. However, relatively low piezoelectric performance restricts their application in detection and conversion of weak mechanical excitations. Herein, wave-shaped 3D piezoelectric device was fabricated by embossing electrospun polyvinylidene fluoride nanofibers. This 3D structured device presents better longitudinal and transverse piezoelectric performance than usual flat-type one. This wave-shaped piezoelectric device was developed for acoustic detection and recognition with a frequency resolution better than 0.1 Hz. This wave-shaped device was capable of frequency spectrum analyses of various sound sources from human and animals and well presents its potential for future wearable acoustic sensors and transducers.

Keywords Piezoelectric polymer · PVDF · Wave-shaped device · Acoustic detection

Introduction

Due to the potential applications of flexible sensors in internet of things and wearable electronics, the demand of highly integrated multifunctional self-powered sensing system is increasing over the past decades. Most of the flexible sensors perceive external stimulation through temperature, humidity, gas, and pressure [1–5], among which pressure sensor

is widely utilized. Pressure sensors are usually classified into piezoelectric [6, 7], piezoresistive [8, 9] and piezocapacitive types [10–12], among which piezoelectric sensors have the advantages of self-power and energy harvesting from environment [13–17]. Usually inorganic piezoelectric materials such as lead zirconate titanate (PZT) ceramic and BaTiO₃ present high piezoelectric coefficient and therefore high sensing and energy harvesting performance [18, 19]. However, inherent inflexibility, brittleness and environmental pollution (such as lead in PZT) hinder their application in wearable electronics [20, 21]. In contrast, piezoelectric polymers such as polyvinylidene fluoride (PVDF) and its copolymer poly(vinylidene fluoride-trifluoroethylene) P(VDF-TrFE) are especially suitable for flexible electronics due to advantages of ease of fabrication, flexibility, biocompatibility and chemical stability [22, 23].

PVDF is well known for its polymorphism [24]. Nonpolar α -phase is the most common and stable phase, while polar β -phase has the highest dipole density. The common measures to transform α -phase to electroactive β -phase include melting re-crystallization [25, 26], mechanical stretching [27, 28], high electrical-field poling [29, 30] and doping

✉ Zaixiu Jiang
zxjiang@tongji.edu.cn

✉ Xiaoqing Zhang
x.zhang@tongji.edu.cn

✉ Guodong Zhu
gdzhu@fudan.edu.cn

¹ Department of Materials Science, Fudan University, Shanghai 200433, China

² Institute of Acoustics, School of Physics Science and Engineering, Tongji University, Shanghai 200092, China

³ Shanghai Key Laboratory of Special Artificial Microstructure Materials and Technology, School of Physics Science and Engineering, Tongji University, Shanghai 200092, China

[31–34]. These measures usually require several processing steps to get polar piezoelectric films. Furthermore, their applicability at a specific circumstance is still to be evaluated. As comparison, electrospinning is an effective technique for one-step fabrication of self-polarized β -phase PVDF nanofiber membranes [35–39].

Flexibility of nanofiber membranes makes them suitable for patterning into desirable geometry according to specific requirement. A dome-shaped piezoelectric polymer sensor detected weak mechanical excitation as low as 25 mN [40]. Deposition of PVDF on wavy substrates effectively enhanced piezoelectric output [41, 42]. Pre-stretching measure was also conducted to prepare wave-shaped piezoelectric composite for wearable application [43]. A energy harvester by attaching PVDF films on an arc-shaped polyimide substrate could light 476 LEDs [44].

As a kind of renewable and ubiquitous energy, acoustic wave widely distributes. However, acoustic energy conversion and detection are not as common as other energy sources because sound pressure is too small to be effectively detected and collected [45]. Integration of a piezoelectric [46] or triboelectric [47] nanogenerator with a Helmholtz resonator could effectively enhance the collection of low-frequency noise. Electrospun PVDF webs with sprayed single-walled carbon nanotubes also presented high acoustic energy conversion efficiency [48]. Selection of proper substrate materials [49] and design of electrode's geometry [14] also improved device's performance.

Herein, electrospun PVDF nanofibers were patterned by embossing templating to form wave-shaped 3D structure. This wave-shaped device has prominent longitudinal and transverse piezoelectric responses and was further used for audible sound detection and recognition. This kind of wave-shaped piezoelectric nanofiber membrane device is a promising candidate for future wearable electronic applications and acoustic sensors.

Experimental Section

Electrospinning of PVDF Nanofibers

PVDF powder ($M_w = 275,000$), *N,N*-dimethylformamide (DMF) ($\geq 99\%$) and acetone were purchased from Sigma Aldrich and used as received. PVDF solution was prepared by dissolving 1.5 g PVDF powder in 10 mL mixture of DMF and acetone (1/1, v/v), stirred at 50 °C for 5 h and then cooled down to room temperature to obtain a homogenous solution.

PVDF nanofibers were fabricated by electrospinning technique (schematic diagram in Fig. 1a). The as-prepared PVDF solution was filled into a plastic syringe with a 27-gauge stainless steel needle. A syringe pump was

used to control the flow rate at 500 $\mu\text{L/h}$. 20 kV voltage was applied to the syringe needle by a high voltage power supply (DW-P303, Tianjin Dongwen, China). An electrically grounded metallic rotating drum (300 rpm rotating speed, 8 cm in diameter, 15 cm in length) covered with an Al foil was used to collect PVDF nanofibers. The distance between needle tip and the collector was 10 cm. An infrared lamp was used to maintain chamber temperature at 50 °C to accelerate evaporation of the organic solvent.

Fabrication of Wave-Shaped Nanofiber Devices

Three kinds of metal templates with periodic and parallel groove structure were employed to fabricate wave-shaped PVDF nanofiber membrane. Typical Dimensions of three templates were listed in Table 1. Those devices obtained from these three templates were labeled as device 1, device 2 and device 3, respectively.

Fabrication process of the wave-shaped PVDF nanofiber devices was schematically illustrated in Fig. 1e (steps I–V). Step I: As-electrospun PVDF membrane, a soft pad and a metal plate were put in sequence on a metal template. Here a soft pad was used to guarantee uniform external pressure. Step II: At room temperature, external pressure of 2 MPa was applied to the top slide to push the PVDF membrane into the template's grooves. The pressure lasted 30 min. Step III: The soft pad, metal plate and PVDF membrane were peeled off in sequence from the metal template, resulting in wave-shaped nanofiber membrane. Step IV: 500 nm thick Al electrodes were vacuum thermally evaporated onto both sides of wave-shaped fibrous membrane. This configuration was used for acoustic sensing and recognition. Step V: As for those devices for piezoelectric performance characterization by using contact-mode mechanical excitation, elastic polydimethylsiloxane (PDMS) was filled onto the bottom grooves of the wave-shaped membrane to guarantee fast strain recovery after removal of the applied excitation.

As a control sample, the as-electrospun PVDF nanofiber membrane was pressed between two flat metal plates and then metal electrodes were vacuum deposited on both sides to form flat-type device.

Structural Characterizations

Morphology of PVDF nanofibers was characterized by scanning electron microscope (SEM, JSM-6701F, JEOL) and crystalline phases were determined by X-ray diffraction (XRD, D8, Bruker Inc).

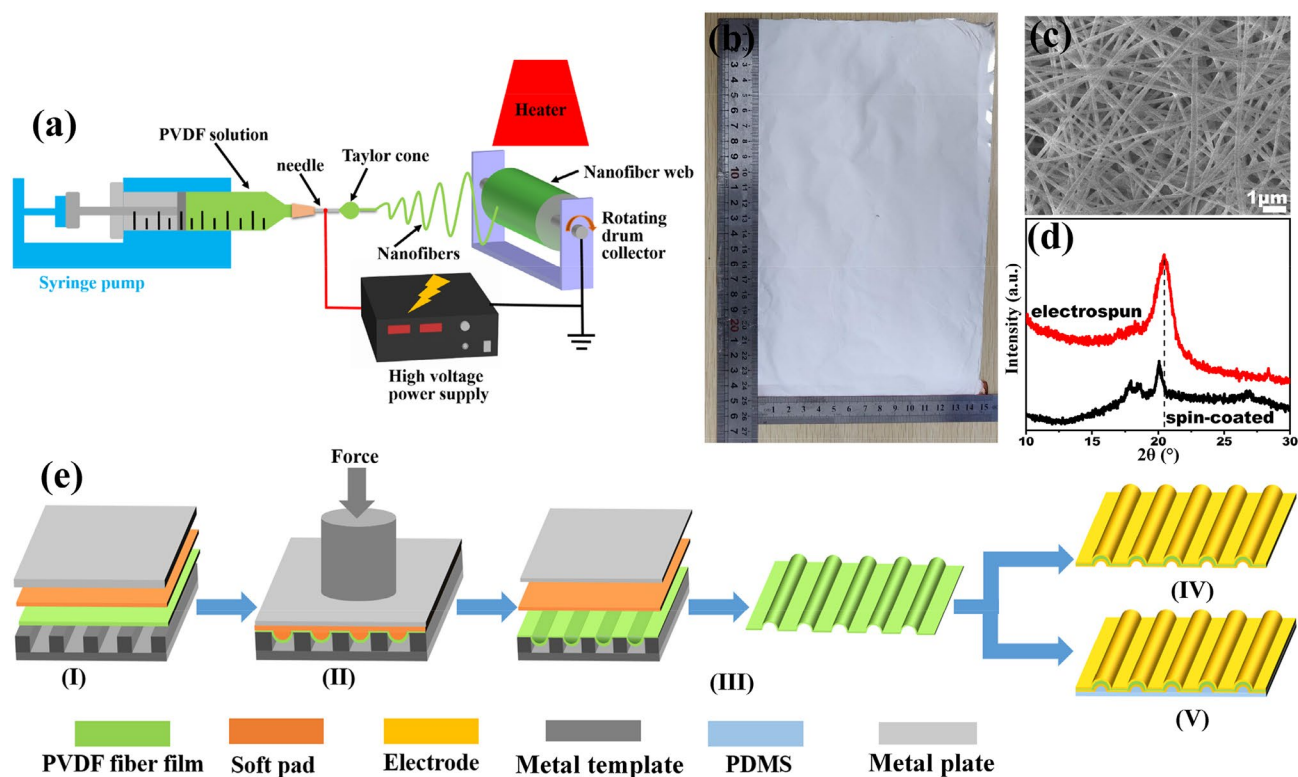


Fig. 1 Fabrication of wave-shaped PVDF nanofiber membrane. **a** Schematic diagram of the electrospinning system. **b** Optical image of a piece of electrospun PVDF nanofiber membrane. **c** SEM and **d**

XRD characterization of the as-electrospun PVDF fiber mat. **e** Schematic diagram of fabrication process of wave-shaped PVDF nanofiber membrane

Table 1 Structures of three kinds of metal templates

Template no.	Groove's height (mm)	Groove's width (mm)	Groove's period (mm)	Corresponding device no.
#1	0.25	0.5	0.75	Device 1
#2	0.5	1.0	1.25	Device 2
#3	0.75	1.5	2.0	Device 3

Piezoelectric Performance Characterization

Both direct longitudinal and transverse piezoelectric properties were determined by home-made measurement system. Here longitudinal piezoelectric property means that the applied strain and the recorded electrical response were both along the Z direction, while transverse piezoelectric property was that strain was applied in X and/or Y directions while electrical response was measured in Z direction.

Longitudinal piezoelectric measurement system was schematically shown in Figure S1. Sinusoidal voltage output from a signal generator was amplified by a power amplifier and then applied to the vibrator to excite its vibration with specific frequency and amplitude. A commercial quartz

force sensor and a nanofiber membrane device were both pressed onto a metal plate fixed on the vibrator. The applied mechanical force was determined according to the induced charges from the quartz sensor which was transformed to voltage signal by a charge amplifier and then recorded by an oscilloscope (Tektronix TBS 1104). The corresponding open-circuit voltage (V_{oc}) and short-circuit current (I_{sc}) outputs from PVDF device were recorded by a sourcemeter (B2902A, Keysight).

Transverse piezoelectric measurement (Figure S2) was performed by fixing both ends of a PVDF fiber membrane on the fixed end and the sliding end of a linear motor, respectively. The reciprocating motion of the slider led to repeated bending of the piezoelectric device, whose electrical output was recorded by a sourcemeter.

Acoustoelectric Conversion Measurement

The wave-shaped PVDF membrane was used as an acoustoelectric conversion device to detect and recognize acoustic signals. A commercial PC loudspeaker (AIBUZ, YLD-714) was used as sound source and controlled by a computer. The piezoelectric membrane was suspended between two PTFE brackets with spacing of 2 cm (Fig. 6a). Acoustic

wave was emitted toward the plane of the fiber membrane. The distance between the sensor and the speaker was fixed at 2 cm. Acoustic frequency and sound pressure level (SPL) were controlled by a computer. SPL was determined by a sound level meter (VICTOR, VC-824). A data acquisition card with a nominal input impedance of 0.5 G Ω (Smacq, USB-3231) was used to record the voltage output from the PVDF sensor.

Results and Discussion

Electrospinning is one convenient and efficient technique for fabrication of large-scale piezoelectric polymer fiber membranes [50–52]. The whole electrospinning system (Fig. 1a) mainly includes a PVDF solution-filled syringe equipped with a metal nozzle, a syringe pump to control flow rate, a high voltage source to bias the nozzle, a rotating drum collector bonded with an Al foil to collect the PVDF nanofiber and an infrared lamp to control environmental temperature. Electronic repulsion between the biased nozzle and the charged polymer solution results in the formation of the so-called Taylor cone in front of the nozzle. Polymer solution jet occurs when electronic repulsion overcomes the viscoelasticity and surface tension of the droplet. During the flight of the droplet toward the grounded Al foil, organic solvent quickly evaporates and PVDF solute gradually solidifies out. The latter is further mechanically stretched in chaotic phase inducing the formation of β -phase nanofibers [53, 54]. According to previous reports, optimal electrospinning parameters are required to avoid the formation of beads. Otherwise, beads can greatly degrade piezoelectric property [14, 55]. In Fig. 1b is shown an optical image of one piece of as-prepared PVDF nanofiber membrane with area as large as 360 cm². The membrane consists of randomly orientated nanofibers with diameter of \sim 200 nm (Fig. 1c) and no unexpected beads occur. XRD spectrum analysis further verifies the formation of electroactive β -phase in electrospun nanofibers (Fig. 1d), whose characteristic diffraction peak occurs at $2\theta = 24.42^\circ$ [56]. As comparison, XRD spectrum from a spin-coated PVDF film present four peaks at $2\theta = 17.83^\circ$, 18.4° , 20.02° , and 26.7° which are mainly attributed to the non-electroactive α -phase [57]. These results indicate that electrospinning technique can realize the fabrication of large-scale and electroactive PVDF nanofiber membrane.

As for the as-prepared PVDF nanofiber membranes, there exists a large number of open pores, which possess much lower elasticity than PVDF nanofibers. Therefore, the deformation of the nanofiber membrane to external mechanical excitation mainly originates from the deformation of these non-electroactive air pores, which doesn't contribute to piezoelectric response. Decrease of pore volume ratio

is expected to improve piezoelectric response [58]. Furthermore, a large number of research work has proved that design of 3D PVDF structure can effectively promote its mechanical and thereafter piezoelectric response to external excitation [41, 43, 44, 59]. Therefore, here the as-prepared electrospun nanofiber membrane is further manufactured by embossing method to form wave-shaped 3D structure. To avoid high temperature induced depolarization, embossing process operates in room temperature. The whole process includes five steps (Fig. 1e). details of fabrication process are described in Experimental part above.

Here three kinds of templates with various grooves' dimensions (Table 1) are used to construct the wave-shaped nanofiber membranes. SEM images of three kinds of wave-shaped PVDF membranes are presented in Fig. 2. Both cross-sectional (Fig. 2a–c) and surface (Fig. 2e–g) images obviously verify the formation of the wave-shaped structure. Dimensions of the embossed PVDF membranes well follow those of the cooper templates. From the magnified section image (Fig. 2d), embossing process results in compact and less porous membrane, though its surface is still covered with disorderly PVDF nanofibers (Fig. 2h).

Mechanical stretching analyses, i.e. tensile stress (σ)-strain (ϵ) curves, were conducted on both flat-type and wave-shaped membranes (Fig. 2i). The wave-shaped PVDF membrane shows break strength of 3.6 MPa and break elongation of 38%, lower than both values of 10.2 MPa and 62% from the flat-type one. Degradation of both values should be attributed to the cold embossing process which, to some extent, results in mechanical damage. Promotion of embossing temperature is expected to decrease this damage. The resultant polarization loss can be compensated by post poling treatment. However, the wave-shaped membrane is much more deformable than the flat one. For example, at the same tensile stress of 1.5 MPa, tensile strain values of the 3D and the flat ones are 21.2% and 3.3%, respectively. Especially, at low strain region ($\epsilon < 15\%$), σ - ϵ curve from the wave-shaped one is slowly ascending with low apparent elastic modulus. Usually large deformation under small stress tends to cause large change in dipole density and therefore induce large electrical response. This mechanical stretching analysis implies that this wave-shaped is especially suitable for detection of weak mechanical excitation.

Mechanical sensing mechanism of this PVDF nanofiber device can be explained according to Figure S3. Since nanofibers are polarized during electrospinning process, inductive charges with opposite polarity occurs on both electrodes (original state in Figure S3a). Compressive stress results in the increase of dipole density in PVDF nanofibers and therefore electrons flow from bottom to top electrodes (Figure S3b). With the increase of compressive stress, more electrons flow to the top electrode until maximum deformation comes (Figure S3c). Then, compressive stress is

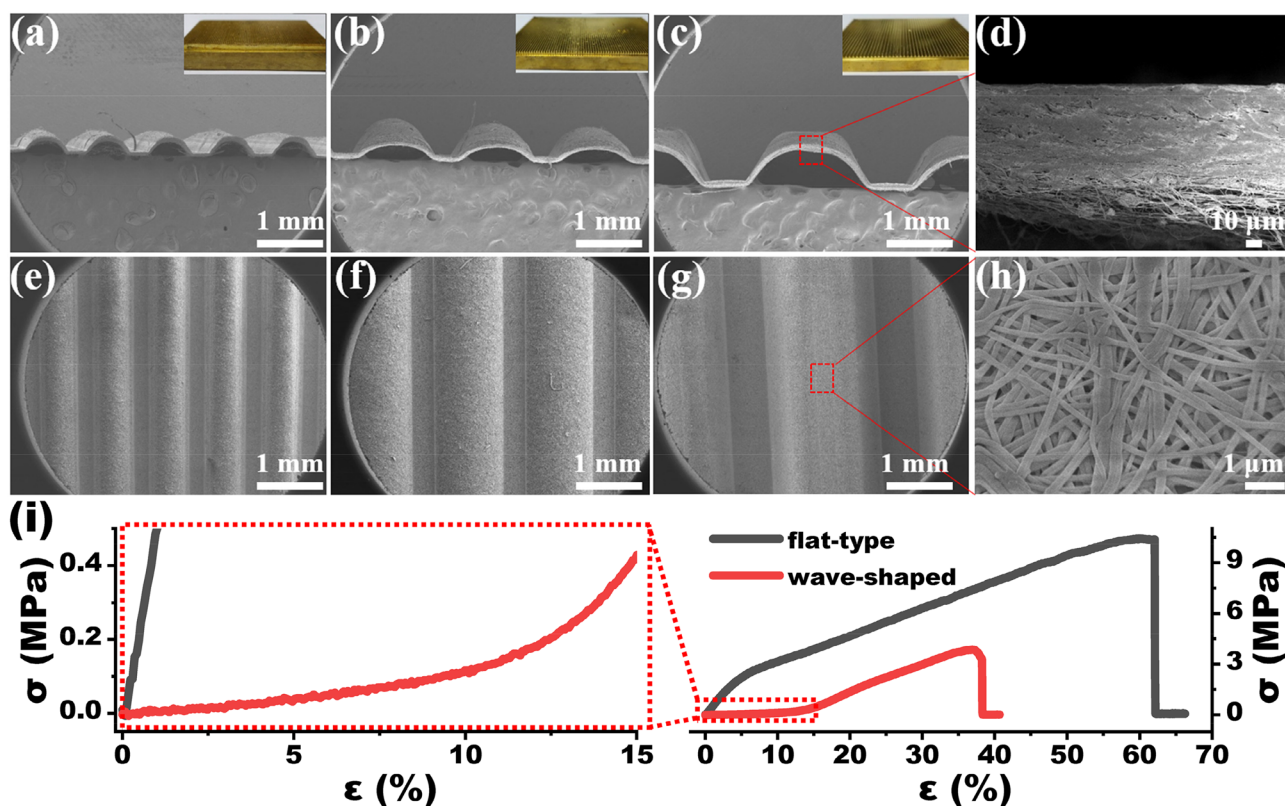


Fig. 2 SEM and mechanical stretching analyses of both flat-type and wave-shaped membranes. SEM images of (a–d) cross-sectional and (e–h) surface morphologies of (a, e) device 1, (b, f) device 2 and (c,

d, g, h) device 3. Insets in figure a–c are the copper templates used to fabricate the wave-shaped structures. i Tensile stress–strain curves of both flat-type and wave-shaped (device 3) fibrous membranes

removed (Figure S2d) and nanofiber membrane tends to recover to its original state. Electrons flow in opposite direction, resulting in the decrease of inductive charge density on both electrodes.

Longitudinal piezoelectric property is characterized via home-designed measurement system (schematic diagram in Figure S1). In Figure S4a and S4b are shown both short-circuit current I_{sc} and open-circuit voltage V_{oc} responses of three kinds of wave-shaped and one flat-type PVDF fiber membranes which are driven by mechanical load with amplitude of 1 N and frequency varying from 1 to 5 Hz. In Fig. 3a, b are plotted the quantitative changes in peak I_{sc} (I_{sc_peak}) and peak V_{oc} (V_{oc_peak}) responses as a function of driving frequency. Obviously, for any PVDF device, its I_{sc} response increases with the increase of driving frequency. This observation is well acceptable since current is the differential of the induced charges with respect to time. Interesting is that the difference in device structure results in difference in both V_{oc} and I_{sc} responses. All three wave-shaped devices present larger I_{sc} and V_{oc} outputs than the flat-type one. Furthermore, with the increase of characteristic dimensions (width and height of the grooves) in wave-shaped devices, I_{sc} and V_{oc} responses increase at any specific driving frequency. For

example, at frequency of 5 Hz, I_{sc_peak} response increases from 2.4, 6.13, 11.63 to 15.58 nA, while V_{oc_peak} response increases from 0.12, 0.19, 0.43 to 0.56 V for the flat-type device and the wave-shaped devices 1 to 3, respectively.

Transverse piezoelectric property of the wave-shaped PVDF nanofiber devices is further determined, since it is of increasing significance in piezoelectric sensing and mechanical energy harvesting applications with the flourishing development of wearable electronics and internet of things, for example, 31-mode cantilever-configured energy harvester [60], recognition of a forefinger's bending [61], and detection of eye fatigue [62]. Both moving velocity V (corresponding to bending frequency) and the maximum displacement L (corresponding to the maximum strain ϵ_{max} that the device suffers) of the sliding end are key factors affecting electrical output of piezoelectric film [60]. In Figure S5 are shown I_{sc} and V_{oc} responses of four PVDF fiber membrane devices when the slider repeatedly moves at different velocities from 7.5 to 30 mm/s while at fixed displacement L of 7.5 mm. To make the results more straightforward, I_{sc_peak} and V_{oc_peak} outputs are extracted and further plotted as a function of bending velocity in Fig. 3c, d. Obviously, I_{sc_peak} tends to increase with the increase of bending velocity, while

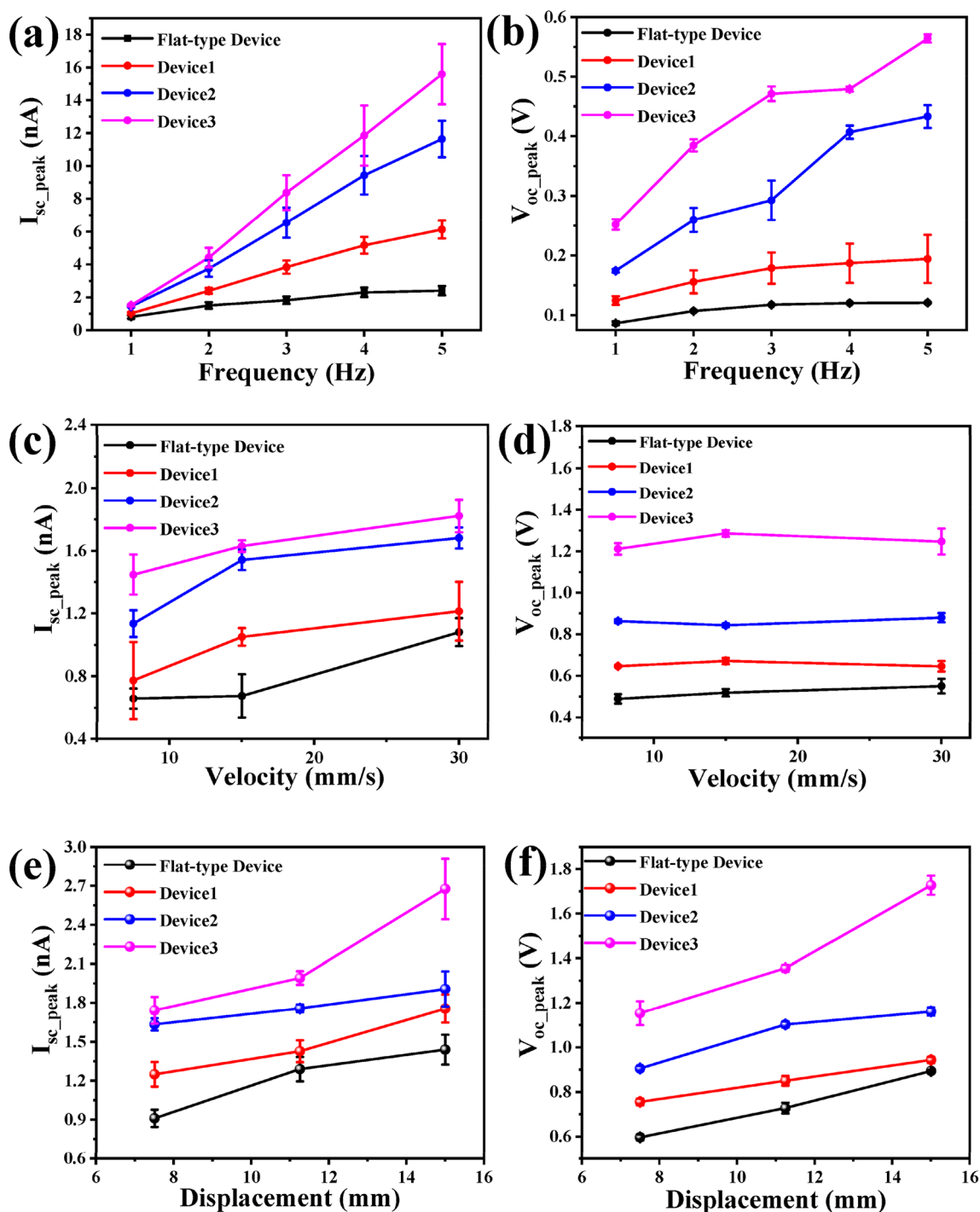


Fig. 3 Quantitative analyses of (a, b) Longitudinal and (c–f) transverse piezoelectric responses from four kinds of PVDF fiber structures. (a, c, e) I_{sc_peak} and (b, d, f) V_{oc_peak} outputs as a function of (a,

b) exciting frequency, (c, d) slider’s moving velocity and (e, f) slider’s maximum displacement. Data in figures a–b, c–d and e–f were extracted from Figure S4, S5 and S6, respectively

V_{oc_peak} is nearly independent of bending velocity. This is reasonable because open-circuit voltage is determined by the deformation, rather than deformation rate [63].

The influence of the maximum slider’s displacement, corresponding to the maximum strain ϵ_{max} of the membrane, on

piezoelectric response is shown in Figure S6 and Fig. 3e–f, where the slider’s velocity is fixed at 22.5 mm/s. Both I_{sc} and V_{oc} responses to repeatedly bending operation are presented in Figure S6. I_{sc_peak} and V_{oc_peak} values are extracted from these results and plotted in Fig. 3e–f. With the increase of

maximum displacement, both I_{sc_peak} and V_{oc_peak} outputs from all four devices increases. Interestingly, I_{sc_peak} and V_{oc_peak} responses from wave-shaped devices are both larger than those from the flat-type device. Furthermore, I_{sc_peak} and V_{oc_peak} values increase with wave structure dimensions, which is consistent with the results from longitudinal piezoelectric property measurement.

In fact, electromechanical enhancement of 3D structured piezoelectric devices has been reported in several publications. The curved structure weakens strain/stress localization and therefore distributes the applied force across the whole piezoelectric surface. In the study of wave-shaped P(VDF-TrFE) devices [43], both theoretical and experimental results show that wave-shaped structure effectively enhanced electromechanical coupling, as is attributed to the synergistic piezoelectric effect of both d_{33} and d_{31} modes, as well as the pre-stretching in P(VDF-TrFE) films, which induced enhancement of effective piezoelectric coefficient. Here cold embossing process also causes pre-stretching in PVDF nanofibers. Therefore, synergistic effect and pre-stretching both contribute to enhanced electric response of our wave-shaped devices. Furthermore, in Fig. 3, the wave-shaped device with the largest characteristic dimensions presents the best electric response to external excitation. Similar phenomenon is also found in near-field electrospun PVDF fibers on sinusoidal surface, where large sinusoidal amplitude corresponded to large electromechanical response [41]. The influence of characteristic dimensions should be due to both large surface area and higher strain experienced during the repeated press/release cycles, which is further verified by finite-element simulation [41].

From those analyses above, the wave-shaped device 3 possesses the best electrical response to external excitation. Therefore, it is further developed as a sensor for acoustic detection and recognition. In Fig. 4a is shown the setup for acoustic detection. Details on system configuration is described in Experimental Section. In Fig. 4b is plotted V_{oc} response to acoustic excitation with frequency of 100 Hz and SPL of 110 dB. V_{oc} value changes between ± 2.8 mV and well follows the acoustic excitation. Both acoustic frequency and SPL influence V_{oc} response of this piezoelectric nanofiber device. In Fig. 4c are shown a series of V_{oc} responses to acoustic excitation at fixed SPL of 110 dB but frequency varying from 40 to 280 Hz. We also submitted a supplementary movie to show how the wave-shaped device works when 70 Hz sound is applied. As comparison, V_{oc} responses to the same excitation from the flat-type device are also plotted in Fig. 4c. To make the results clearer, quantitative peak-to-peak V_{oc} (V_{oc_pp}) values are collected and drawn as a function of sound frequency in Fig. 4d. There are two characteristics. One is that, for a specific sound frequency, V_{oc_pp} response from the wave-shaped device is always larger than that from the flat-type one. For example, at 100 Hz,

V_{oc_pp} output from device 3 is 5.51 mV, much larger than that of 3.25 mV from the flat-type device. This observation further verifies the high sensitivity of this 3D structured sensor. The other is that, for both devices, V_{oc_pp} response sharply degrades once sound frequency is higher than 200 Hz. This result should be attributed to the suspended device structure, which induces mechanical resonance under lower frequency range. Besides, both acoustic sensors are sensitive to low and medium frequency sound waves. It is known that frequency range of human hearing is about 20–20,000 Hz [64, 65]. In industrial and public transport areas, sound frequency is usually between 40 and 200 Hz [14]. Therefore, this wave-shaped acoustic sensor presents potential in these areas. However, it is necessary to emphasize that, though the device presents high response at low sound frequency range, it still responds to sound waves at higher frequency.

SPL is another important parameter that greatly influence electrical response of both kinds of devices. Typical SPL dependence of V_{oc_pp} response is plotted in Fig. 4e. During measurement, sound frequency is maintained at 100 Hz. V_{oc_pp} response from both devices increases with SPL. Again, at any specific SPL value, V_{oc_pp} response from device 3 is still higher than that from the flat-type one. With the increase of SPL from 80 to 120 dB, V_{oc_pp} value increases from 0.7 to 5.57 mV for the device 3, while it increases from 0.27 to 3.28 mV for the flat-type one.

Frequency spectrum analysis is one basic function of acoustic sensors, which requires good frequency recognition ability, i.e. the capability to distinguish tiny difference between two close acoustic frequencies. To confirm this capacity of our wave-shaped device, a mixing sound wave with two determinate frequencies was generated by the computer and then emitted by the loudspeaker. Typical V_{oc} responses of this 3D structured device are presented in Fig. 5a, b, and their corresponding FFT (fast Fourier transformation) spectrum analyses are plotted in Fig. 5c. Note that here FFT spectra are obtained by offline, rather than real-time, FFT analysis via a professional software (OriginPro here). The waveform of V_{oc} response changes with the difference of the sound frequency, as implies its capacity to track acoustic signals. FFT frequency spectra in Fig. 5c further emphasizes its excellent ability to recognize different sounds with tiny frequency difference. In our measurement, a frequency difference as small as 0.1 Hz can be precisely distinguished (the FFT spectrum of the mixture of 100 Hz and 100.1 Hz sound waves). Two peaks in this FFT spectrum correspond exactly to 100 Hz and 100.1 Hz, well consistent with the nominal sound frequencies. With the further decrease of the frequency difference to 0.01 Hz (the result from 100 and 100.01 Hz sound mixture), FFT spectrum still presents two peaks of 99.96 Hz and 100.01 Hz. The divergence between the nominal 100 Hz and the recorded 99.96 Hz may be due to

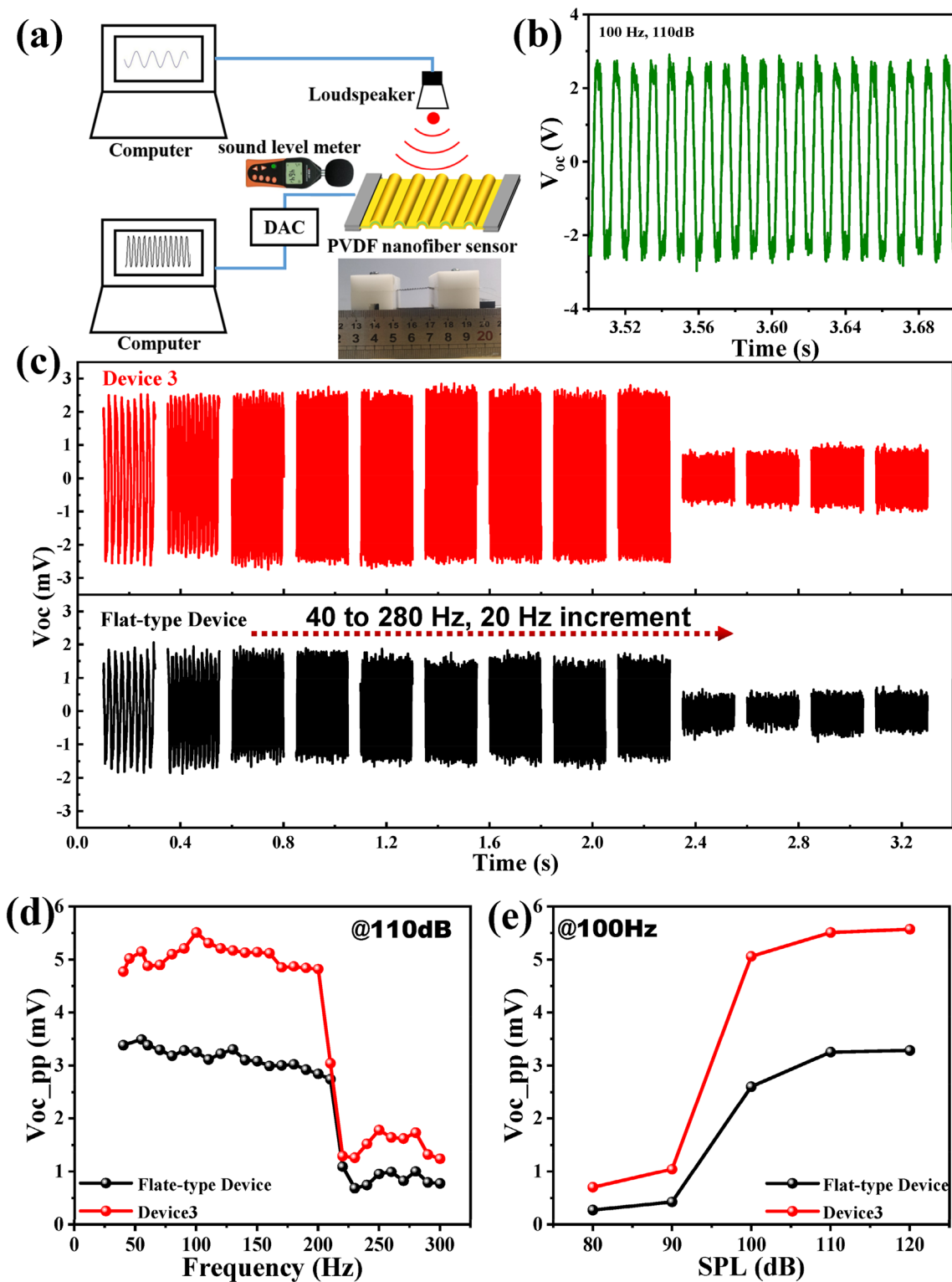


Fig. 4 Acoustic detection by both flat-type and wave-shaped sensors. **a** Schematic diagram of the acoustic detection system. **b** V_{oc} response of one wave-shaped device 3 to acoustic excitation with frequency of

100 Hz and SPL of 110 dB. **c** V_{oc} response of both devices to acoustic excitation with SPL of 110 dB and varied frequency. **d** Sound frequency and **e** SPL dependence of V_{oc_pp} responses from both devices

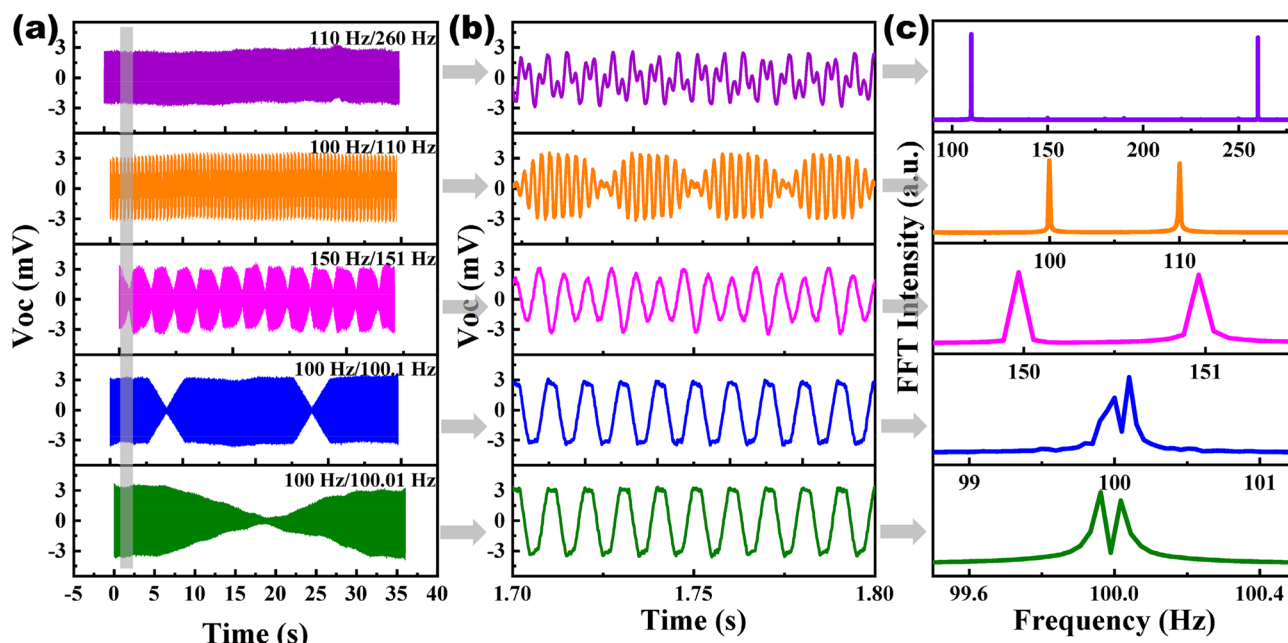


Fig. 5 Sound frequency recognition of device 3. **a** V_{oc} response to acoustic excitation whose frequency spectrum is a mixture of two frequencies. Both frequency values are labeled on top right corner of

each sub-image. **b** Local magnification of V_{oc} responses in **a**. **c** FFT analyses of those recorded V_{oc} response curves in **a**. During these measurements, SPL was maintained at 100 dB

(1) original sound frequency error from the computer and the loudspeaker or (2) relatively low sampling rate of the data acquisition card used here. Currently we cannot judge which factor contributes most to this divergence. Anyway, this wave-shaped device presents good frequency resolution and is comparable to the reported PVDF nanofiber sensor with through hole structure [14].

This high-performance acoustic sensor can be used for sound detection and recognition. In Fig. 6a, b are shown the V_{oc} responses and the corresponding FFT frequency spectra of a male volunteer's voice when he pronounced numbers in order from 'one' to 'ten'. Every pronunciation has its own frequency spectrum characteristic between 100 and 1200 Hz. Additionally, since everyone's voice has his unique frequency spectrum characteristic, this wave-shaped acoustic sensor is expected to be used for human identification according to characteristic acoustic frequency spectrum. In Fig. 6c, d are shown the V_{oc} responses and the corresponding FFT frequency spectra when a male volunteer pronounced seven musical notes (Do, Re, Mi, Fa, Sol, La, Xi). As comparison, in Fig. 6e, f are V_{oc} responses and the corresponding FFT spectra when a female volunteer pronounced these notes. The difference in V_{oc} amplitude reflects the difference of acoustic strength between male and female. Furthermore, the male volunteer's frequency spectra are more complicated and most of peaks lie in low frequency range between 80 and 800 Hz. However, acoustic frequency from a female volunteer mainly occurs between 400 and 1300 Hz. This

observation is well acceptable since a female's voice usually includes more high frequency information.

Since this wave-shaped nanofiber sensor is capable of acoustic detection with high fidelity, it also shows potential in environmental protection and biometrics. In Fig. 7a, b are shown the detection and recognition of seven kinds of animal sounds (tiger, dog, wolf, cock, cat, duck, and eagle). Animal sound sources were collected through the internet and emitted via the loudspeaker. Each animal has its own characteristic frequency spectrum. Frequency spectra of some animals are well consistent with those collected by an in-situ polarized P(VDF-TrFE) film [66]. This result implies that this 'sound fingerprint' is one promising measure for animal recognition.

Conclusions

In summary, here we reported a wave-shaped piezoelectric nanofiber device for acoustic detection and recognition. Electrospun PVDF nanofiber membrane was further patterned by embossing method to realize this kind of 3D wave-shaped structure. The wave-shaped nanofiber device presented better longitudinal and transverse piezoelectric performance than the usual flat-type piezoelectric nanofiber device. This 3D device could effectively distinguish acoustic frequency difference of at least 0.1 Hz and realize frequency spectrum analyses of various acoustic

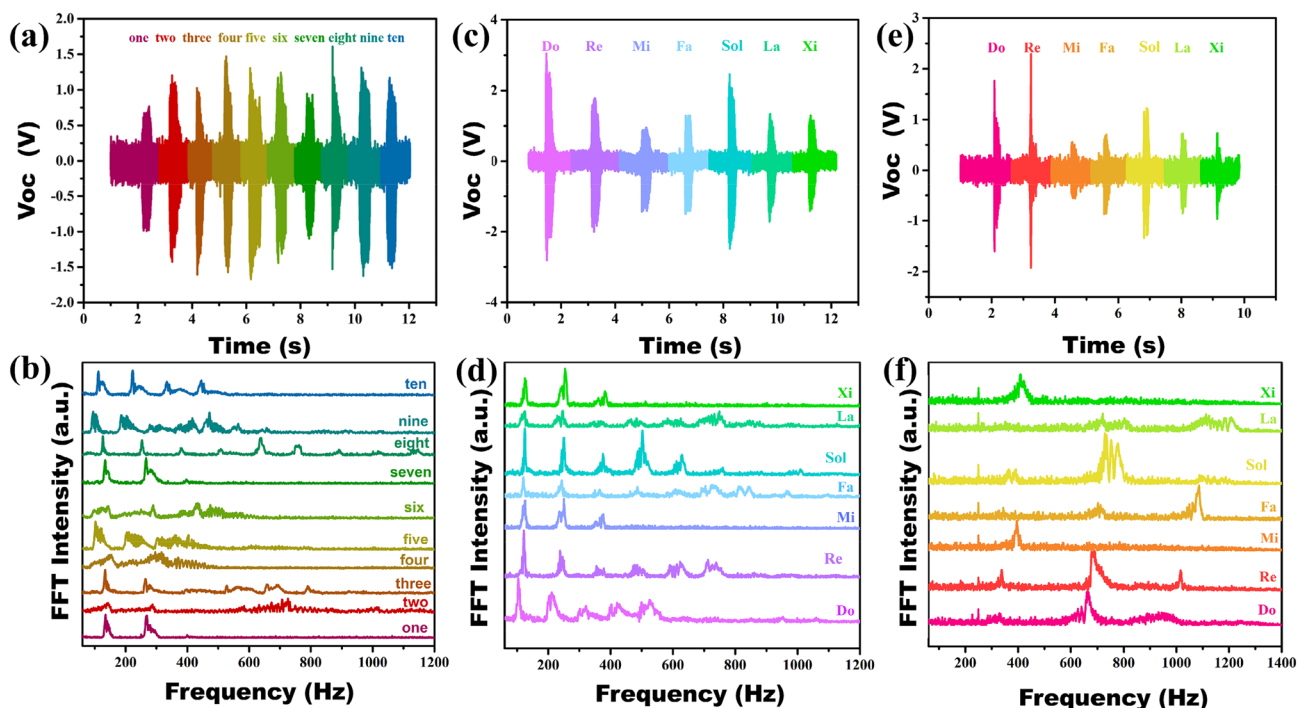


Fig. 6 Frequency spectrum analyses of volunteers' voice by the wave-shaped device 3. **a** V_{oc} responses **b** the corresponding FFT analyses of a volunteer's sound when he pronounces from 'one' to 'ten' in order.

c–f V_{oc} responses to **c** a male volunteer's and **e** a female volunteer's pronunciation of seven musical notes (Do, Re, Mi, Fa, Sol, La, Xi) and **d, f** their corresponding FFT analyses

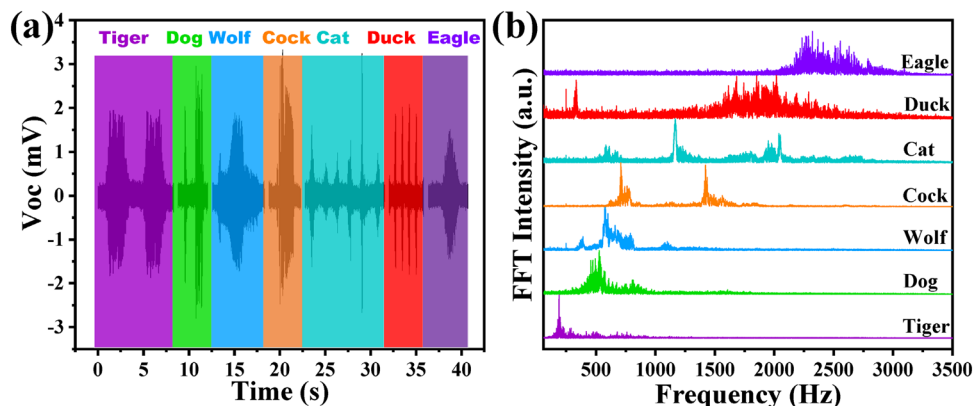


Fig. 7 Frequency spectrum analyses of animals' sounds

sources from human and animals. These results prove that this kind of wave-shaped piezoelectric nanofiber device is a promising candidate for future wearable acoustic sensors and transducers.

Supplementary Information The online version contains supplementary material available at <https://doi.org/10.1007/s42765-021-00095-7>.

Acknowledgements This work was financially supported by the Science and Technology Commission of Shanghai Municipality (STCSM, Grant No. 21520711600 and 20ZR1408200) and the National Natural Science Foundation of China (NSFC, Grant No. 61774043).

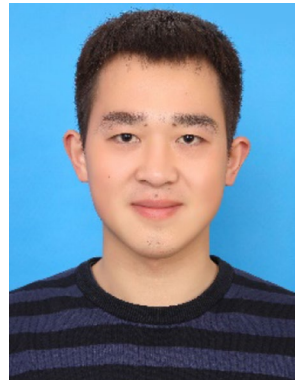
Declarations

Conflict of interest The authors declare that they have no conflict of interest.

References

- Ma M, Guo L, Anderson DG, Langer R. Bio-inspired polymer composite actuator and generator driven by water gradients. *Science*. **2013**;339:186.
- Wei W, Gao J, Yang J, Wei J, Guo J. A NIR light-triggered piezoelectric-dominated generator based on a liquid crystal elastomer composite actuator for photoelectric conversion and self-powered sensing. *RSC Adv*. **2018**;8:40856.
- Zhou H, Zhang Y, Qiu Y, Wu H, Qin W, Liao Y, Yu Q, Cheng H. Stretchable piezoelectric energy harvesters and self-powered sensors for wearable and implantable devices. *Biosens Bioelectron*. **2020**;168:112569.
- Zhou J, Fei P, Gao Y, Gu Y, Liu J, Bao G, Wang ZL. Mechanical-electrical triggers and sensors using piezoelectric microwires/nanowires. *Nano Lett*. **2008**;8:2725.
- Nazemi H, Joseph A, Park J, Emadi A. Advanced micro-and nanogas sensor technology: A review. *Sensors*. **2019**;19:1285.
- Hosseini ES, Manjakkal L, Shakthivel D, Dahiya R. Glycine-chitosan-based flexible biodegradable piezoelectric pressure sensor. *ACS Appl Mater Interfaces*. **2020**;12:9008.
- Nguyen DN, Moon W. Piezoelectric polymer microfiber-based composite for the flexible ultra-sensitive pressure sensor. *J Appl Polym Sci*. **2020**;137:48884.
- Shi J, Wang L, Dai Z, Zhao L, Du M, Li H, Fang Y. Multi-scale hierarchical design of a flexible piezoresistive pressure sensor with high sensitivity and wide linearity range. *Small*. **2018**;14:1800819.
- Yu R, Xia T, Wu B, Yuan J, Ma L, Cheng GJ, Liu F. Highly sensitive flexible piezoresistive sensor with 3D conductive network. *ACS Appl Mater Interfaces*. **2020**;12:35291.
- Ma L, Shuai X, Hu Y, Liang X, Zhu P, Sun R, Wong C-P. A highly sensitive and flexible capacitive pressure sensor based on a micro-arrayed polydimethylsiloxane dielectric layer. *J Mater Chem C*. **2018**;6:13232.
- Kim H, Kim G, Kim T, Lee S, Kang D, Hwang MS, Chae Y, Kang S, Lee H, Park HG. Transparent, flexible, conformal capacitive pressure sensors with nanoparticles. *Small*. **2018**;14:1703432.
- Pignatelli J, Schlingman K, Carmichael TB, Rondeau-Gagné S, Ahamed MJ. A comparative analysis of capacitive-based flexible PDMS pressure sensors. *Sens Actuator A Phys*. **2019**;285:427.
- Lee S, Bae SH, Lin L, Yang Y, Park C, Kim SW, Cha SN, Kim H, Park YJ, Wang ZL. Super-flexible nanogenerator for energy harvesting from gentle wind and as an active deformation sensor. *Adv Funct Mater*. **2013**;23:2445.
- Lang C, Fang J, Shao H, Ding X, Lin T. High-sensitivity acoustic sensors from nanofibre webs. *Nat Commun*. **2016**;7:1.
- Yang Y, Zhang H, Lin Z-H, Zhou YS, Jing Q, Su Y, Yang J, Chen J, Hu C, Wang ZL. Human skin based triboelectric nanogenerators for harvesting biomechanical energy and as self-powered active tactile sensor system. *ACS Nano*. **2013**;7:9213.
- Zeng W, Tao X-M, Chen S, Shang S, Chan HLW, Choy SH. Highly durable all-fiber nanogenerator for mechanical energy harvesting. *Energy Environ Sci*. **2013**;6:2631.
- Wang J, Ding W, Pan L, Wu C, Yu H, Yang L, Liao R, Wang ZL. Self-powered wind sensor system for detecting wind speed and direction based on a triboelectric nanogenerator. *ACS Nano*. **2018**;12:3954.
- Wu W, Bai S, Yuan M, Qin Y, Wang ZL, Jing T. Lead zirconate titanate nanowire textile nanogenerator for wearable energy-harvesting and self-powered devices. *ACS Nano*. **2012**;6:6231.
- Pi Z, Zhang J, Wen C, Zhang Z-B, Wu D. Flexible piezoelectric nanogenerator made of poly (vinylidene fluoride-co-trifluoroethylene) (PVDF-TrFE) thin film. *Nano Energy*. **2014**;7:33.
- Wen X, Wu W, Ding Y, Wang ZL. Piezotronic effect in flexible thin-film based devices. *Adv Mater*. **2013**;25:3371.
- Wang Z, Hu J, Suryavanshi AP, Yum K, Yu M-F. Voltage generation from individual BaTiO₃ nanowires under periodic tensile mechanical load. *Nano Lett*. **2007**;7:2966.
- Kawai H. The piezoelectricity of poly (vinylidene fluoride). *Jpn J Appl Phys*. **1969**;8:975.
- Chen X, Han X, Shen QD. PVDF-based ferroelectric polymers in modern flexible electronics. *Adv Electron Mater*. **2017**;3:1600460.
- Lovinger AJ. Ferroelectric polymers. *Science*. **1983**;220:1115.
- Wang J, Li H, Liu J, Duan Y, Jiang S, Yan S. On the α - β transition of carbon-coated highly oriented PVDF ultrathin film induced by melt recrystallization. *J Am Chem Soc*. **2003**;125:1496.
- Pan H, Na B, Lv R, Li C, Zhu J, Yu Z. Polar phase formation in poly (vinylidene fluoride) induced by melt annealing. *J Polym Sci Pol Phys*. **2012**;50:1433.
- Sencadas V, Moreira MV, Lanceros-Méndez S, Pouzada AS, Gregório Filho R. α -to β transformation on PVDF films obtained by uniaxial stretch. *Mater Sci Forum*. **2006**;872:514–516. <https://doi.org/10.4028/www.scientific.net/MSF.514-516.872>
- Sencadas V, Gregorio R Jr, Lanceros-Méndez S. α to β phase transformation and microstructural changes of PVDF films induced by uniaxial stretch. *J Macromol Sci*. **2009**;48:514.
- Davis G, McKinney J, Broadhurst M, Roth S. Electric-field-induced phase changes in poly (vinylidene fluoride). *J Appl Phys*. **1978**;49:4998.
- Li M, Wondergem HJ, Spijckman M-J, Asadi K, Katsouras I, Blom PW, De Leeuw DM. Revisiting the δ -phase of poly (vinylidene fluoride) for solution-processed ferroelectric thin films. *Nat Mater*. **2013**;12:433.
- Kang SJ, Park YJ, Bae I, Kim KJ, Kim HC, Bauer S, Thomas EL, Park C. Printable ferroelectric PVDF/PMMA blend films with ultralow roughness for low voltage non-volatile polymer memory. *Adv Funct Mater*. **2009**;19:2812.
- Shah D, Maiti P, Gunn E, Schmidt DF, Jiang DD, Batt CA, Gianellis EP. Dramatic enhancements in toughness of polyvinylidene fluoride nanocomposites via nanoclay-directed crystal structure and morphology. *Adv Mater*. **2004**;16:1173.
- Yu S, Zheng W, Yu W, Zhang Y, Jiang Q, Zhao Z. Formation mechanism of β -phase in PVDF/CNT composite prepared by the sonication method. *Macromolecules*. **2009**;42:8870.
- Garain S, Jana S, Sinha TK, Mandal D. Design of in situ poled Ce³⁺-doped electrospun PVDF/graphene composite nanofibers for fabrication of nanopressure sensor and ultrasensitive acoustic nanogenerator. *ACS Appl Mater Interfaces*. **2016**;8:4532.
- Baji A, Mai Y-W, Li Q, Liu Y. Electrospinning induced ferroelectricity in poly (vinylidene fluoride) fibers. *Nanoscale*. **2011**;3:3068.
- Liu Z, Pan C, Lin L, Huang J, Ou Z. Direct-write PVDF nonwoven fiber fabric energy harvesters via the hollow cylindrical near-field electrospinning process. *Smart Mater Struct*. **2013**;23:025003.
- Persano L, Dagdeviren C, Su Y, Zhang Y, Girardo S, Pisignano D, Huang Y, Rogers JA. High performance piezoelectric devices based on aligned arrays of nanofibers of poly (vinylidene fluoride-co-trifluoroethylene). *Nat Commun*. **2013**;4:1.
- Ma S, Ye T, Zhang T, Wang Z, Li K, Chen M, Zhang J, Wang Z, Ramakrishna S, Wei L. Highly oriented electrospun P (VDF-TrFE) fibers via mechanical stretching for wearable motion sensing. *Adv Mater Technol*. **2018**;3:1800033.

39. Chang C, Tran VH, Wang J, Fuh Y-K, Lin L. Direct-write piezoelectric polymeric nanogenerator with high energy conversion efficiency. *Nano Lett.* **2010**;10:726.
40. Li C, Wu P-M, Lee S, Gorton A, Schulz MJ, Ahn CH. Flexible dome and bump shape piezoelectric tactile sensors using PVDF-TrFE copolymer. *J Microelectromech Syst.* **2008**;17:334.
41. Fuh YK, Wang BS, Tsai C-Y. Self-powered pressure sensor with fully encapsulated 3D printed wavy substrate and highly-aligned piezoelectric fibers array. *Sci Rep.* **2017**;7:6759.
42. Zhao J, You Z. A shoe-embedded piezoelectric energy harvester for wearable sensors. *Sensors.* **2014**;14:12497.
43. You S, Shi H, Wu J, Shan L, Guo S, Dong S. A flexible, wave-shaped P (VDF-TrFE)/metglas piezoelectric composite for wearable applications. *J Appl Phys.* **2016**;120:234103.
44. Jung W-S, Lee M-J, Kang M-G, Moon HG, Yoon S-J, Baek S-H, Kang C-Y. Powerful curved piezoelectric generator for wearable applications. *Nano Energy.* **2015**;13:174.
45. Cui N, Gu L, Liu J, Bai S, Qiu J, Fu J, Kou X, Liu H, Qin Y, Wang ZL. High performance sound driven triboelectric nanogenerator for harvesting noise energy. *Nano Energy.* **2015**;15:321.
46. Wang Y, Zhu X, Zhang T, Bano S, Pan H, Qi L, Zhang Z, Yuan Y. A renewable low-frequency acoustic energy harvesting noise barrier for high-speed railways using a Helmholtz resonator and a PVDF film. *Appl Energy.* **2018**;230:52.
47. Zhao H, Xiao X, Xu P, Zhao T, Song L, Pan X, Mi J, Xu M, Wang ZL. Dual-tube helmholtz resonator-based triboelectric nanogenerator for highly efficient harvesting of acoustic energy. *Adv Energy Mater.* **2019**;9:1902824.
48. Hwang YJ, Choi S, Kim HS. Highly flexible all-nonwoven piezoelectric generators based on electrospun poly (vinylidene fluoride). *Sens Actuator A Phys.* **2019**;300:111672.
49. Lee B-S, Park B, Yang H-S, Han JW, Choong C, Bae J, Lee K, Yu W-R, Jeong U, Chung U-I. Effects of substrate on piezoelectricity of electrospun poly (vinylidene fluoride)-nanofiber-based energy generators. *ACS Appl Mater Interfaces.* **2014**;6:3520.
50. Li B, Zhang F, Guan S, Zheng J, Xu C. Wearable piezoelectric device assembled by one-step continuous electrospinning. *J Mater Chem C.* **2016**;4:6988.
51. You S, Zhang L, Gui J, Cui H, Guo S. A flexible piezoelectric nanogenerator based on aligned P (VDF-TrFE) nanofibers. *Micromachines.* **2019**;10:302.
52. Fang J, Niu H, Wang H, Wang X, Lin T. Enhanced mechanical energy harvesting using needleless electrospun poly (vinylidene fluoride) nanofiber webs. *Energy Environ Sci.* **2013**;6:2196.
53. Reneker DH, Yarin AL. Electrospinning jets and polymer nanofibers. *Polymer.* **2008**;49:2387.
54. Lei T, Cai X, Wang X, Yu L, Hu X, Zheng G, Lv W, Wang L, Wu D, Sun D. Spectroscopic evidence for a high fraction of ferroelectric phase induced in electrospun polyvinylidene fluoride fibers. *RSC Adv.* **2013**;3:24952.
55. Lang C, Fang J, Shao H, Wang H, Yan G, Ding X, Lin T. High-output acoustoelectric power generators from poly (vinylidene fluoride-co-trifluoroethylene) electrospun nano-nonwovens. *Nano Energy.* **2017**;35:146.
56. Andrew J, Clarke D. Enhanced ferroelectric phase content of polyvinylidene difluoride fibers with the addition of magnetic nanoparticles. *Langmuir.* **2008**;24:8435.
57. Martins P, Lopes A, Lanceros-Mendez S. Electroactive phases of poly (vinylidene fluoride): Determination, processing and applications. *Prog Polym Sci.* **2014**;39:683.
58. Yang L, Zhao Q, Chen K, Ma Y, Wu Y, Ji H, Qiu J. PVDF-based composition-gradient multilayered nanocomposites for flexible high-performance piezoelectric nanogenerators. *ACS Appl Mater Interfaces.* **2020**;12:11045.
59. Jung W-S, Lee M, Baek S-H, Jung IK, Yoon S-J, Kang C-Y. Structural approaches for enhancing output power of piezoelectric polyvinylidene fluoride generator. *Nano Energy.* **2016**;22:514.
60. Liu H, Zhong J, Lee C, Lee S-W, Lin L. A comprehensive review on piezoelectric energy harvesting technology: Materials, mechanisms, and applications. *Appl Phys Rev.* **2018**;5:041306.
61. Jiang H, Yang J, Xu F, Wang Q, Liu W, Chen Q, Wang C, Zhang X, Zhu G. VDF-content-guided selection of piezoelectric P (VDF-TrFE) films in sensing and energy harvesting applications. *Energy Convers Manage.* **2020**;211:112771.
62. Lü C, Wu S, Lu B, Zhang Y, Du Y, Feng X. Ultrathin flexible piezoelectric sensors for monitoring eye fatigue. *J Micromech Microeng.* **2018**;28:025010.
63. Yang J, Chen Q, Xu F, Jiang H, Liu W, Zhang X, Jiang Z, Zhu G. Epitaxy enhancement of piezoelectric properties in P (VDF-TrFE) copolymer films and applications in sensing and energy harvesting. *Adv Electron Mater.* **2020**;6:2000578.
64. Vollandri G, Di Puccio F, Forte P, Carmignani C. Biomechanics of the tympanic membrane. *J Biomech.* **2011**;44:1219.
65. Leventhall HG. Low frequency noise and annoyance. *Noise Health.* **2004**;6:59.
66. Guo Z, Liu S, Hu X, Zhang Q, Shang F, Song S, Xiang Y. Self-powered sound detection and recognition sensors based on flexible polyvinylidene fluoride-trifluoroethylene films enhanced by in-situ polarization. *Sens Actuator A Phys.* **2020**;306:111970.



Fan Xu received his M.S. degree from Jiangsu University of Science and Technology (2017) and Ph.D. degree from Fudan University (2021), respectively. His main research interest includes piezoelectric sensing and energy harvesting.



Zaixiu Jiang received his Ph.D. degree from Tongji University in 2006 and then joined the faculty of Tongji University as lecturer. His research interests include noise simulation, noise control and novel acoustic materials.



Xiaoqing Zhang received her Ph.D. degree in Condensed Matter Physics from Tongji University, China in 2001. From April 2001 to December 2004, she was as a postdoctoral fellow, working on the dielectric properties of the inorganic dielectric materials and the piezoelectric properties of the polymer films, at Darmstadt University of Technology, Germany. She has been a full professor and the leader of the research group of Electrets and Functional Dielectrics at Tongji University since December

2010. Her interests are electro-active materials and their applications. She has over 100 scientific publications and holds 16 patents. She is a co-editor of the *European Journal of Electrical Engineering (EJEE)*, a member of the academic committees of the IEEE International Conference on Electrets, the International Conference on Vibration and Energy Harvesting Applications, and Chinese National Conference on Electrets. She is a senior IEEE member.



Guodong Zhu received his B.S. (2000) and Ph.D. (2005) degrees in condensed matter physics from Tongji University, China. He joined the department of Materials Science in Fudan University in 2005 and was promoted associate professor in 2007. He was a visiting scholar of the Electrical Engineering Department at UCLA during 2011. After that he has been a full professor with Fudan University. His research interest focuses on flexible electronic materials and devices. Since

2016 Zhu has been member of academic committee of the Chinese National Conference on Electrets.